Article

Quantifying Soil Moisture Impacts on Water Use Efficiency in Terrestrial Ecosystems of China

Xingming Hao [1,2,*] **, Jingjing Zhang** [1,2,3] **, Xue Fan** [2,4] **, Haichao Hao** [1,2,3] **and Yuanhang Li** [2,4]

1   State Key Laboratory of Desert and Oasis Ecology, Xinjiang Institute of Ecology and Geography, Chinese Academy of Sciences, 818 South Beijing Road, Urumqi 830011, China; zhangjingjing19@mails.ucas.ac.cn (J.Z.); 18235153557@139.com (H.H.)
2   Akesu National Station of Observation and Research for Oasis Agro-Ecosystem, Akesu 843017, China; fanxue961@163.com (X.F.); 18337672237@139.com (Y.L.)
3   School of Chemistry and Chemical Engineering, University of Chinese Academy of Sciences, Beijing 100049, China
4   College of Life Sciences, Xinjiang Normal University, Urumqi 830054, China
*   Correspondence: haoxm@ms.xjb.ac.cn; Tel.: +86-991-7823056; Fax: +86-991-7823174

Abstract: Soil moisture (*SM*) significantly affects the exchange of land surface energy and the stability of terrestrial ecosystems. Although some conclusions have been drawn about the effects of *SM* on the ecosystem water use efficiency (*WUE*), the influence mechanism and the quantitative assessment framework of *SM* on *WUE* are still unclear. This study provides an analysis framework for the feedback relationship between *SM* and *WUE* based on the dependence of the evaporation fraction on *SM* and output datasets from remote sensing and the Global Land Data Assimilation System. The results show that the range of *WUE* of terrestrial ecosystems of China was 0.02–19.26 g C/kg H$_2$O in the growing season with an average value of 1.05 g C/kg H$_2$O. They also show a downward trend in 43.99% of the total area. In the evapotranspiration (*ET*) pathway, SM negatively affected *WUE*, and the sensitivity coefficient ranged from −18.49 to −0.04. In the net primary production (*NPP*) pathway, the sensitivity coefficient ranged from −68.66 to 43.19. Under the dual effects of the *ET* and *NPP* pathways, the influence of *SM* on *WUE* was negative in 84.62% of the area. Variation in *SM* led to significant *WUE* variability. Generally, the percentage change in *WUE* (Δ*WUE*) ranged from 0% to 190.86%, with an average value of 28.02%. The maximum Δ*WUE* ranged from 0% to 758.78%, with an average value of 109.29%. The *WUE* of forest ecosystems showed strong resistance to *SM* variation, whereas that of non-forest vegetation was more sensitive to *SM* variation. This analytical framework provides a new perspective on the feedback relationship between *WUE* and *SM* in terrestrial ecosystems.

Keywords: feedback relationship; evaporation fraction; net primary production (NPP); elasticity coefficient; climatic zone

1. Introduction

The water use efficiency (*WUE*) of an ecosystem is the ratio of carbon sequestration to water consumption, which couples the terrestrial carbon and water cycles and closely links photosynthesis and evapotranspiration (*ET*) processes in the ecosystem [1,2]. Although there are many ways to express the *WUE* of an ecosystem, the ratio of the net primary production (*NPP*) to *ET* is widely used [3]. The variation of *WUE* controlled by both biotic and abiotic factors [4,5] and recent research showed that a vapor pressure deficit (*VPD*) and canopy conductance are two dominant factors of *WUE* in response to drought [6]. On the global scale, *WUE* is positively related with drought in the majority of regions [7]. In China, most forest ecosystems exhibit strong drought resistance by improving their *WUE* [8]. Under the influence of the negative feedback relationship between *ET* and air temperature [9,10], the variation in *WUE* is usually positively correlated with air

temperature [11]. Many studies have shown that, in the past 30 years, the vegetation cover, gross primary productivity (*GPP*) and *ET* in western China have been low, and the demand for evaporation has been high [12]. In the context of climate change, many studies focus on the response process and mechanism of *WUE* to the constraints of drought or water conditions [7,13,14]. On a global scale, *WUE* generally decreases with an increase in drought or geographic latitude [15]. However, studies have shown that *WUE* generally has a positive relationship with the drought degree. Drought events can slightly increase the *WUE* in the majority of forest, grassland, and shrub ecosystems [16,17]. In addition, the response of the *WUE* to drought has spatial heterogeneity at different spatial scales and in different ecosystems. *ET* has been shown to control the *WUE* response to drought in semi-arid and high-latitude regions, and *GPP* dominated the response *WUE* to drought in tropical forest regions [7]. Thus, a quantitative study of *WUE* and its spatial variation along drought gradients is essential for understanding the regional environmental and physiological functions of heterogeneous landscapes [16,18].

As an important indicator of drought, soil moisture (*SM*) often plays a vital role in the ecosystem carbon–water relationship [19–22]. Studies have shown that *SM* can indirectly affect the *WUE* of terrestrial ecosystems by controlling the *NPP* and *ET* processes [21]. Soil water loss in sub-humid, semi-arid, and arid regions can reduce the total primary productivity by 40% [23]. Granier et al. showed that when the soil relative extractable water (*REW*) was below 0.4, the *GPP* decreased significantly and the total ecosystem respiration did not decrease until the *REW* continued to decrease to 0.2 [24]. However, another study showed that because water stress has less limitation on carbon assimilation than *ET*, *ET* decreases especially on cloudy days, thereby resulting in a significant increase in *WUE* [25]. In the global forest ecosystem, the variations in ecosystem *WUE*, *GPP*, and *ET* are correlated with *SM*, and the sensitivities of the *WUE* to the soil water content significantly increase with the increase in the vapor pressure deficit [26]. The seasonal fluctuation of *SM* caused by local rainfall is the main factor determining the *GPP/ET* relationship in the tropical Amazon rainforest [27,28].Given the above results, some studies think that soil water use efficiency is an adequate representative and indicator of *WUE* [15,29]. Therefore, studying the influence mechanism of *SM* on *WUE* is of great significance to the evolution of terrestrial ecosystems and the response to climate change.
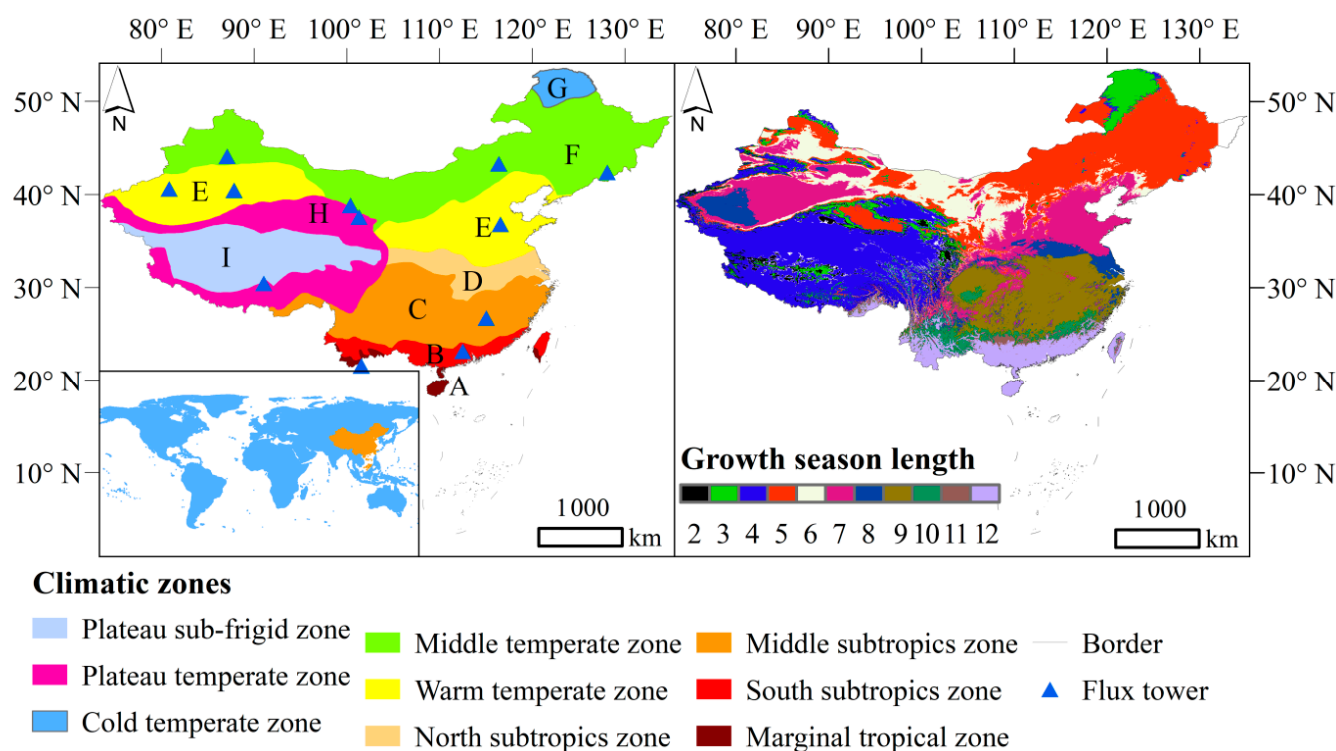
Many studies have shown that a decrease in soil moisture or an increase in drought severity usually increases the *WUE* [7,25,30,31]. A recent study showed that *SM*, rather than *VPD*, dominates dryness stress on ecosystem production globally [32]. Considering *SM* can better reflect the *ET* rate at a large regional scale [33,34], *ET* often dominates the *WUE* variability in arid and semi-arid regions [7]. Therefore, whether from *NPP* or *ET* pathways, *SM* should be the dominant factor affecting *WUE*. However, the influencing mechanism by which *SM* variability affects *WUE* is still unclear. Soil water variation has a dual effect on the *WUE* by affecting both *NPP* and *ET*. However, current research on the quantitative analysis of this complex process is insufficient. Thus, this study focuses on three questions: (1) What were the spatiotemporal variation characteristics of *WUE* in the terrestrial ecosystems of China over the past 30 years (1985–2014)? (2) What is the cause and effect mechanism by which *SM* influences *WUE* and how can it be quantitatively evaluated? (3) To what extent does the variation of *SM* affect *WUE*?

2. Materials and Methods

2.1. Study Area

China has a land area of approximately 9.6×10^6 km^2 and diverse ecosystems. According to the vegetation map of China (1:1,000,000), grassland ecosystems account for the largest proportion of terrestrial ecosystems, covering 29.88% of the total land area, followed by forest ecosystems, which cover for 23.96% of the total land area. In addition, farmland, desert, wetland, and other ecosystems accounted for 18.82%, 13.53%, 3.92%, and 7.55% of the total land area, respectively.

This study mainly discussed the variation in *WUE* and *SM* in different climate zones of the terrestrial ecosystem. The terrestrial ecosystem in China has eight climatic zones, namely, the marginal tropical zone (A), south subtropics zone (B), middle subtropics zone (C), north subtropics zone (D), warm temperate zone (E), middle temperate zone (F), cold temperate zone (G), temperate zone in Qinghai–Tibet Plateau (H), and sub-frigid zone in Qinghai–Tibet Plateau (I) (Figure 1). As the terrestrial ecosystems of China span multiple climatic zones, its climatic growth seasons also have significant spatial differences, ranging from the shortest two-month growth season to the longest twelve-month growth season (Figure 1).

Figure 1. Sketch map of climatic zones (**left**)and the length of growing seasons (**right**) in the terrestrial ecosystemsof China.

2.2. Data

Monthly latent heat flux (*LE*), sensible heat flux (*H*) and ground heat flux (*G*), *ET*, surface net radiation (R_n), and *SM* (four layers: 0–10, 10–40, 40–100, 100–200 cm) datasets were obtained from the NASA Global Land Data Assimilation System (GLDAS) Noah model (GLDAS_NOAH025_M_2.0). We used the dataset from 1985 to 2014 with a spatial resolution of $0.25° \times 0.25°$ (downloaded from https://disc.gsfc.nasa.gov/datasets, accessed on 10 October 2020). In this study, *SM* in the 0–100 cm soil layer was regarded as the *SM* of root zone based on previous research [35,36]. The monthly *NPP* dataset (spatial resolution of 1 km $\times$ 1 km) of China's terrestrial ecosystems north of 18°N from 1985 to 2014 was obtained from the Global Change Research Data Publishing & Repository of China. The *NPP* data were calculated using the Carnegie–Ames–Stanford Approach (CASA) model based on the monthly meteorological data of China's land from 1985 to 2015, national soil texture data, and land cover and vegetation index data from the Moderate Resolution Imaging Spectroradiometer (MODIS) and the Advanced Very High Resolution Radiometer (AVHRR) remote sensing images. CASA model is a process-based remote sensing model for estimating *NPP* of terrestrial ecosystem, which is driven by grid datasets of climate, radiation, soil, and remote sensing vegetation index [37]. A comparative analysis with the measured and simulated data from previous studies [38–42] showed that the *NPP* dataset used in this study hadgood accuracy [43].

To verify the *NPP* and *ET* (GLDAS) data, this study collected the monthly observation data from eight flux towers in China from 2003 to 2010, which were provided by ChinaFLUX (http://www.cnern.org.cn/, accessed on 15 September 2021). In addition, this study also collected the monthly observation flux data from the other four flux towers from the stations, and the collected data length of these four stations was 2004–2006, 2011–2014, 2008–2011, and 2013–2014, respectively. This study also used *SM* data based on microwave remote sensing in China from 2002 to 2011 (provided by the National Tibetan Plateau Data Center (TPDC) of China; http://data.tpdc.ac.cn, accessed on 2 August 2021) to verify the *SM* data from GLDAS. The spatial and temporal resolutions of the *SM* dataset (from the TPDC) were 0.25° and monthly, respectively. The dataset was calculated based on the high spatial and temporal resolution surface meteorological dataset and an improved land surface assimilation system to drive the Simple Biosphere model (SiB2) and assimilate the brightness temperature observed by the Advanced Microwave Scanning Radiometer Earth Observing System sensor (AMSR-E) satellite [44,45]. The verifications showed that the RMSE of this SM dataset (from the TPDC) was approximately 5% volumetric soil water content [45,46].

The soil texture dataset was obtained from the TPDC of China (http://data.tpdc.ac.cn, accessed on 13 May 2020). The dataset was calculated based on the 1:1,000,000 scale soil map and 8595 soil profiles of China's second national soil survey and the regional land and climate simulation standard of the U.S. Department of Agriculture (soil texture classification standard is shown in Table 1). This study also used the data of soil hydraulic properties in China, which were provided by the National Cryosphere Desert Data Center of China (http://www.crensed.ac.cn/portal/, accessed on 21 August 2020).

Table 1. Soil texture classification standard of soil texture dataset.

		Soil Diameter (mm)						
>3	**3~2**	**2~1**	**1~0.5**	**0.5~0.25**	**0.25~0.1**	**0.1~0.05**	**0.05~0.002**	**<0.002**
rock	gravel	sand					silt	clay
		very coarse sand	coarse sand	medium sand	fine sand	very fine sand		

This study extracted the growing season by using the base temperature threshold of 10 °C (≥10 °C) [47] based on the multi-year monthly average air temperature. The required grid data of monthly average temperature in China (1985–2014) were downloaded from the "National Tibetan Plateau Data Center" of China (http://data.tpdc.ac.cn, accessed on 13 May 2020). However, in the Qinghai Tibet Plateau, the maximum monthly average temperature in most areas is usually lower than 10 °C. Therefore, according to the local actual situation and previous studies [48,49], the growth season was defined as June to September.

2.3. Methods

2.3.1. Mathematical Expression between *SM* and *EF*

Previous studies have proposed an effective analysis method for the functional relationship between the evaporation fraction (*EF*) and *SM* [50,51]. This method expressed the dependence of *EF* on *SM* (θ) as follows:

$$EF(\theta)\begin{cases} 0, & \text{if } \theta < \theta_{\text{r}} \\ EF_{\max}\frac{\theta-\theta_{\text{r}}}{\theta_{\text{c}}-\theta_{\text{r}}}, & \text{if } \theta_{\text{r}} \leq \theta \leq \theta_{\text{s}} \\ EF_{\max}, & \text{if } \theta > \theta_{\text{s}} \end{cases} \tag{1}$$

where θ is volumetric soil moisture content (m^3/m^3), θ_c is the soil moisture at the critical point, and θ_r is the soil wilting coefficient. *EF* is the evaporative fraction, which is calculated as follows:

$$EF = \frac{LE}{R_n} \qquad (2)$$

where *LE* is the latent heat flux and R_n is the surface net radiation. When $\theta < \theta_r$, *EF* is not always zero owing to the presence of hygroscopic *SM* [52]. Therefore, EF_{min} is defined as the *EF* value corresponding to a cumulative frequency percentage of 5%. In addition, when $\theta > \theta_c$, energy rather than *SM* became the dominant limiting factor for *ET*. Thus, the study similarly defined EF_{max} as the *EF* value corresponding to 95% of the cumulative frequency percentage. Because this study only focused on the functional relationship between *SM* and *EF* in the range of $EF_{min} \leq EF \leq EF_{max}$, Equation (1) could be expressed as follows:

$$\theta = \frac{EF}{EF_{max}}(\theta_c - \theta_r) + \theta_r \qquad (3)$$

This study estimated the raster map of θ_r using soil hydraulic parameters and soil texture datasets [53]. Although the fitting between *EF* and θ could obtain the parameter θ_c, it could result in great uncertainty. Thus, this study used the soil field capacity (θ_f) to replace θ_c and introduced a dimensionless parameter A into the calculation scheme for correction. Finally, Equation (3) was deformed as follows:

$$\theta = \frac{EF}{EF_{max}} A(\theta_f - \theta_r) + \theta_r \qquad (4)$$

The gridded θ_f value was also calculated using soil hydraulic parameters and soil texture datasets [53]. First, we used the monthly *SM* and *EF* data from 1985 to 2000 to fit the multi-year average monthly (January to December) parameter A. Then, the monthly *SM* from 2001 to 2014 was estimated using the *EF* data during the same period and the fitted parameter A. The GLDAS *SM* data finally verified the estimated soil moisture data during 2001–2014.

2.3.2. The Response of *WUE* to *SM* Variation

Generally, *WUE* is calculated as follows:

$$WUE = \frac{NPP}{ET} \qquad (5)$$

Based on Equation (2), *ET* could be expressed as follows:

$$ET = \frac{R_n \times EF}{L} \qquad (6)$$

where *L* is the latent heat of vaporization, which is the ratio of *LE* to *ET*. Thus, the elasticity of *WUE* to the variation of *SM* could be divided into two contributions based on Equations (4) to (6), as follows:

$$\frac{\partial WUE}{\partial \theta} = \frac{\partial WUE}{\partial ET}\frac{\partial ET}{\partial \theta} + \frac{\partial WUE}{\partial NPP}\frac{\partial NPP}{\partial \theta} \qquad (7)$$

The first term on the right side of the equation describes the impact of *SM* variation on the *ET* process and the further influence on the *WUE*. This term was calculated based on Equations (3), (5) and (6). The second term on the right of the equation is the sensitivity of *WUE* to *SM* variation via the *NPP* pathway, which was estimated based on Equation (5) and the following statistical method:

$$\varepsilon = \text{median}\left[\frac{(NPP_i - \overline{NPP})/\overline{NPP}}{(\theta_i - \overline{\theta})/\overline{\theta}}\right] \qquad (8)$$

where ε is the sensitivity coefficient; $\overline{NPP}$ and $\overline{\theta}$ are the long-term average values of the *NPP* and *SM* in growing season of a pixel; NPP_i and θ_i are the growing season values of *NPP* and *SM* in each year, respectively.

Thus, the following formula could be used to evaluate the average impact of *SM* variation on *WUE* in the past 30 years:

$$\Delta WUE = \left| \frac{\partial WUE}{\partial \theta} \right| \Delta\theta \tag{9}$$

where $\Delta\theta$ is the percentage change in *SM* in the growing season from 1985 to 2014. Thus, ΔWUE was the average influence (change percentage) of *SM* variation on *WUE*. Similarly, the impact of the maximum variation of *SM* on *WUE* was calculated as follows:
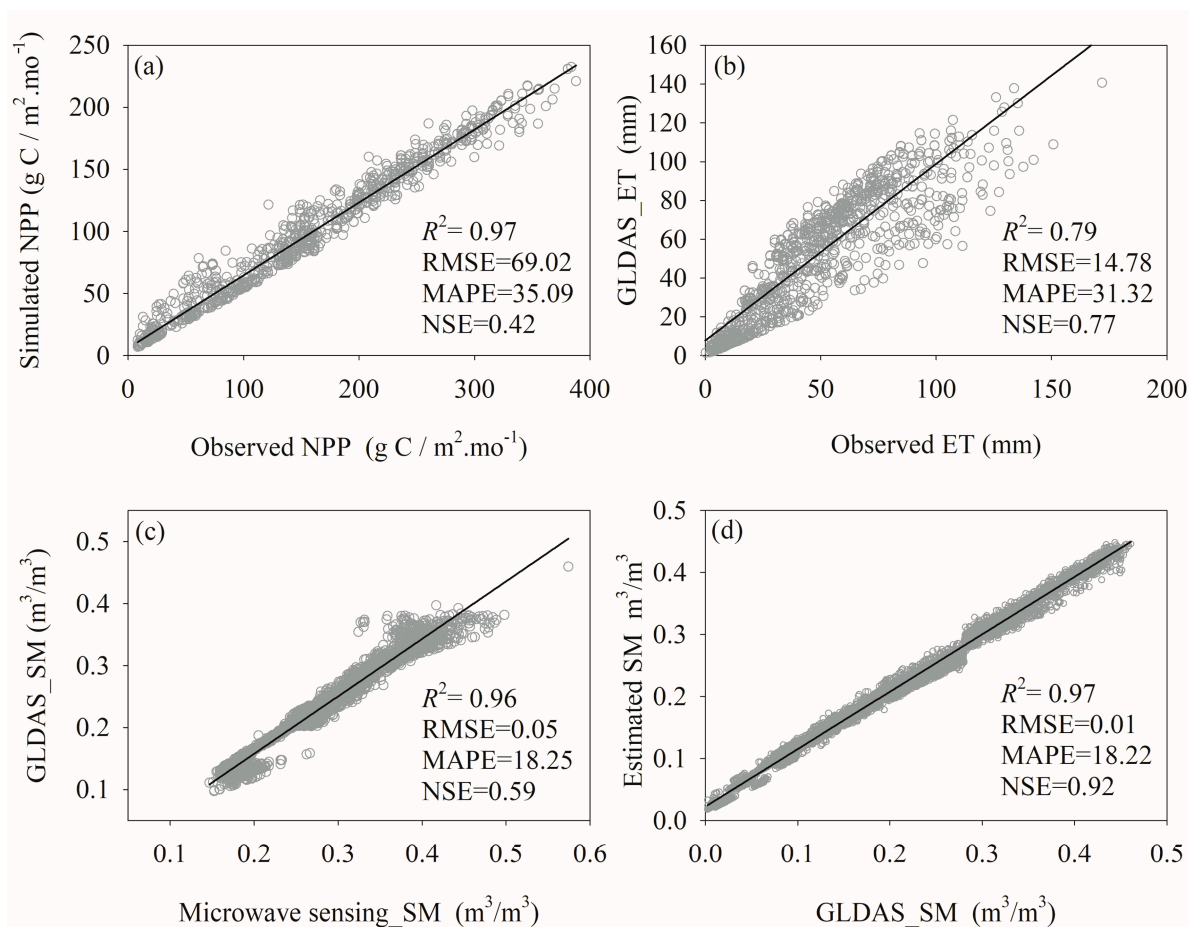
$$\Delta WUE_{\max} = \left| \frac{\partial WUE}{\partial \theta} \right| \Delta\theta_{\max} \tag{10}$$

where $\Delta\theta_{\max}$ is the maximum rate of change in *SM* during the growing season from 1985 to 2014, which was calculated as the difference between the maximum and minimum values of *SM* during the period. $\Delta WUE_{\max}$ is the maximum possible impact of *SM* variation on *WUE* during the growing season in past 30 years.

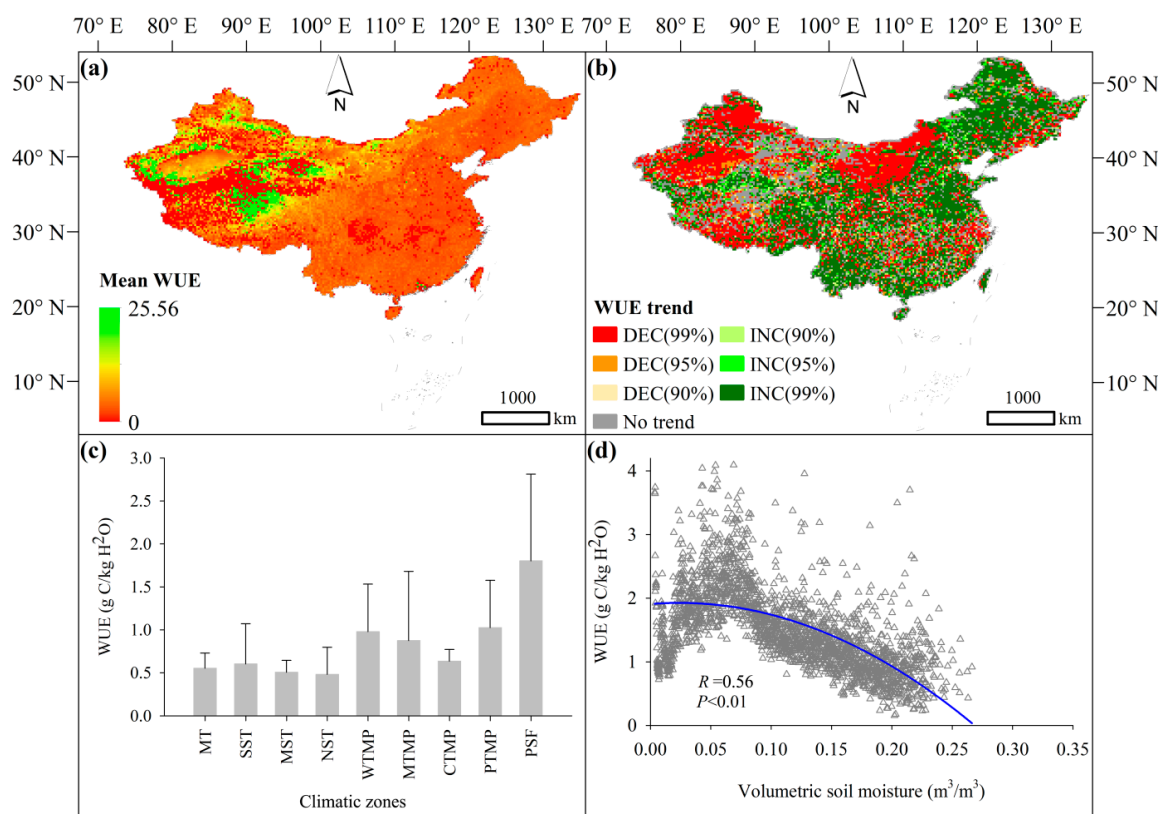## 3. Results

3.1. Data Verification

The analysis of this study was based on the output datasets of the climate model and remote sensing model, including the *ET* and *SM* datasets from GLDAS, and the *NPP* dataset from the Global Change Research Data Publishing & Repository of China. The verification results showed that the monthly *ET* of the GLDAS dataset and the observed *ET* data in 12 flux towers in China had a good consistence (Figure 2b). The determination coefficient (R^2), root mean square error (RMSE), mean absolute percent error (MAPE), and Nash–Sutcliffe efficiency coefficient (NSE) between the simulated and measured *ET* values were 0.79, 14.78 mm, 31.32%, and 0.77, respectively. In addition, the verification results of *NPP* data showed that, although the estimated monthly *NPP* data used in this study underestimated the actual *NPP*, the R^2, RMSE, MAPE, and NSE between the estimations and observations were 0.97, 69.02 g $C \cdot m^{-2} \cdot mo^{-1}$, 35.09%, and 0.42, respectively, which indicated that the *NPP* dataset used in this study was also consistent with the observations (Figure 2a). This study compared the *SM* data based on microwave remote sensing data assimilation in China (2002–2011) with GLDAS *SM* data (Figure 2c), owing to the lack of measured *SM* data. The results showed a good consistency, and the R^2, RMSE, MAPE, and NSE values were 0.96, 0.05 $m^3 \cdot m^{-3}$, 18.25%, and 0.59, respectively. Furthermore, The monthly *SM* from 2001 to 2014 was estimated using Equation (4) and then verified using *SM* data of GLDAS. The overall trend of change in estimated *SM* was close to the GLDAS *SM* data, and the determination coefficient (R^2) was 0.97 (Figure 2d). Meanwhile, the RMSE, MAPE, and NSE of this simulation were 0.01 $m^3 \cdot m^{-3}$, 18%, and 0.92, respectively. The fitting error was primarily due to the overestimation of *SM*, especially when the *SM* was low. This study may have overestimated *SM* in some arid regions or during dry seasons. Although there were still some simulation errors, the datasets used in this study were generally reliable and could ensure the accuracy of the results.

Figure 2. Accuracy verification of net primary production (*NPP*), evapotranspiration (*ET*), and soil moisture data used in this study. (**a**) Scatter plot between the estimated and measured monthly *NPP* from 12 flux towers from 2003 to 2010; (**b**) scatter plot between the monthly *ET* data from the Global Land Data Assimilation System (GLDAS) dataset and the measured monthly *ET* data from 12 flux towers from 2003 to 2010; (**c**) scatter plot between the monthly volumetric soil moisture in the root zone (0–100 cm soil layer) from the GLDAS dataset and the *SM* dataset based on microwave sensing from 2002 to 2011; (**d**) scatter plot between the estimated (in this study) and GLDAS soil moisture data in the root zone (0–100 cm soil layer) of the study area.

3.2. Spatiotemporal Variation of WUE

In terms of the growing season, the range of *WUE* in all terrestrial ecosystems was 0.02–19.26 g C/Kg H_2O, with an average value of 1.05 g C/Kg H_2O and a standard deviation of 1.45 g C/Kg H_2O. Furthermore, the high-value areas of *WUE* were mainly located in the arid regions of Northwest China (Figure 3a). The spatial variation in *WUE* in the different climatic zone was also distinct (Figure 3c). The sub-frigid zone in the Qinghai–Tibet Plateau(PSF) and the temperate zone in the Qinghai–Tibet Plateau (PTMP) had the highest *WUE*, with maximum values of 1.80 g C/Kg H_2O and 1.03 g C/Kg H_2O, respectively. The north subtropics (NST) had the lowest *WUE* with a value of 0.48 g C/Kg H_2O. The *WUE* in the warm temperate zone (WTMP), middle temperate zone (MTMP), cold temperate zone (CTMP), south subtropics zone (SST),marginal tropical(MT) zone, and middle subtropics zone (MST) was0.98, 0.87, 0.64, 0.60, 0.55, and 0.51 g C/Kg H_2O, respectively. In general, the change in *WUE* was correlated with the *SM* (coefficient of determination: *R* = 0.56), and a higher *SM* usually led to a lower WUE (Figure 3d).

Figure 3. Temporal and spatial variation characteristics of water use efficiency (*WUE*) in the terrestrial ecosystems of China during the growing season from 1985 to 2014. (**a**) Multi-year average *WUE* in the growing season; (**b**) Mann–Kendall test of the *WUE* change trend ("DEC" is the decrease trend and "INC" is the increase trend) in the growing season; (**c**) multi-year average *WUE* in the growing season in different climatic zones, whiskers indicate standard deviation; (**d**) scatter plot between *WUE* and *SM* in the growing season, and the blue solid line is the change trend of fitted by quadratic curve. The abbreviations of MT, SST, MST, NST, WTMP, MTMP, CTMP, PTMP, and PSF represent the marginal tropical zone, south subtropics zone, middle subtropics zone, north subtropics zone, warm temperate zone, middle temperate zone, cold temperate zone, temperate zone in Qinghai–Tibet Plateau, and the sub-frigid zone in Qinghai–Tibet Plateau (PSF), respectively.
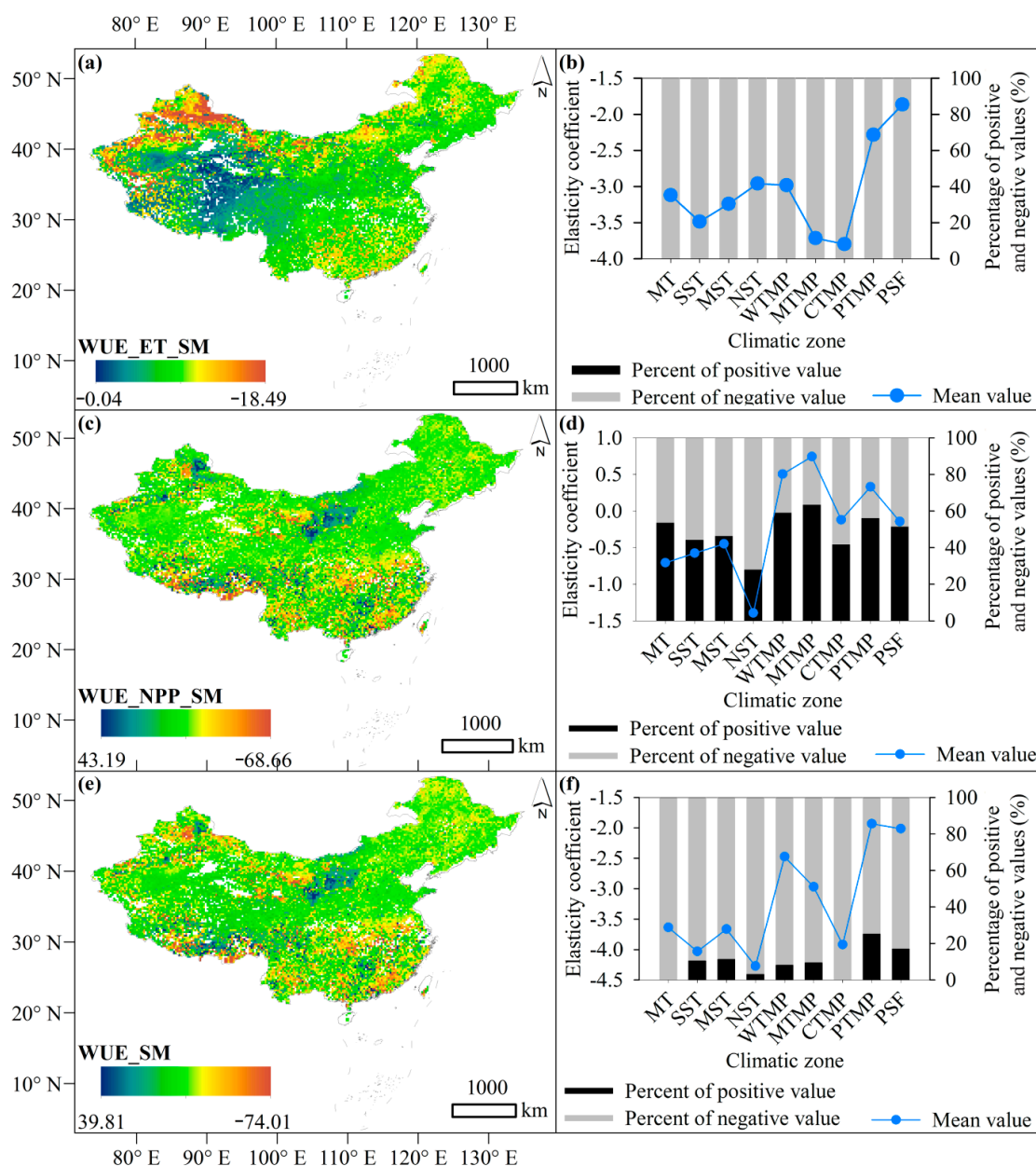
During the growing season, *WUE* showed a downward trend in 43.99% of the total area. Among these areas, *WUE* showed extremely significant (Sig = 0.99), significant (Sig = 0.95), and insignificant (Sig = 0.90) downward trends in 35.03%, 6.11%, and 2.58% of the total terrestrial ecosystem area, respectively. In contrast, *WUE* also showed an increasing trend in 34.91% of the total area of the terrestrial ecosystem. Among these areas, the percentage with extremely significant, significant, and insignificant increases in *WUE* was 28.07%, 4.94% and 1.91%, respectively. Thus, in the past 30 years, the *WUE* of the terrestrial ecosystem has generally shown a downward trend, especially in the arid areas of Northwest China, the Mongolian Plateau, and the southern Qinghai–Tibet Plateau. *WUE* also showed a significant downward trend in some areas of the monsoon region of China (Figure 3b).

3.3. Elasticity of WUE to SM

The variation in *SM* can, simultaneously, directly affect the *NPP* and *ET*, which, ultimately, leads to the changes in *WUE*. On the *ET* pathway, the sensitivity coefficient of the *WUE* to *SM* ($\frac{\partial WUE}{\partial ET} \frac{\partial ET}{\partial \theta}$) at the growing season scale ranged from -18.49 to -0.04, with an average of -3.02 (Figure 4a). Generally, the negative impact of *SM* on *WUE* via the *ET* pathway in the arid region of northwestern China was the most significant, followed by that in the southeast monsoon region. The impact in the central China region was relatively

insignificant. This negative effect (Figure 4b) was mainly due to the negative feedback relationship between the *WUE* and *ET* (EF). In different climatic zones, the negative impact of *SM* on *WUE* via the *ET* pathway was the lowest in the PSF, and the average value of the elasticity coefficient was −1.87. The impact was the most significant in the CTMP, with an average elasticity coefficient being −3.80. In other zones, the adverse effects of *SM* on *WUE* via the *ET* pathway were in the order of MTMP, SST, MST, MT, WTMP, NST, and PTMP, with average elasticity coefficients of −3.72, −3.49, −3.24, −3.12, −2.98, −2.96, and −2.29, respectively (Figure 4b).
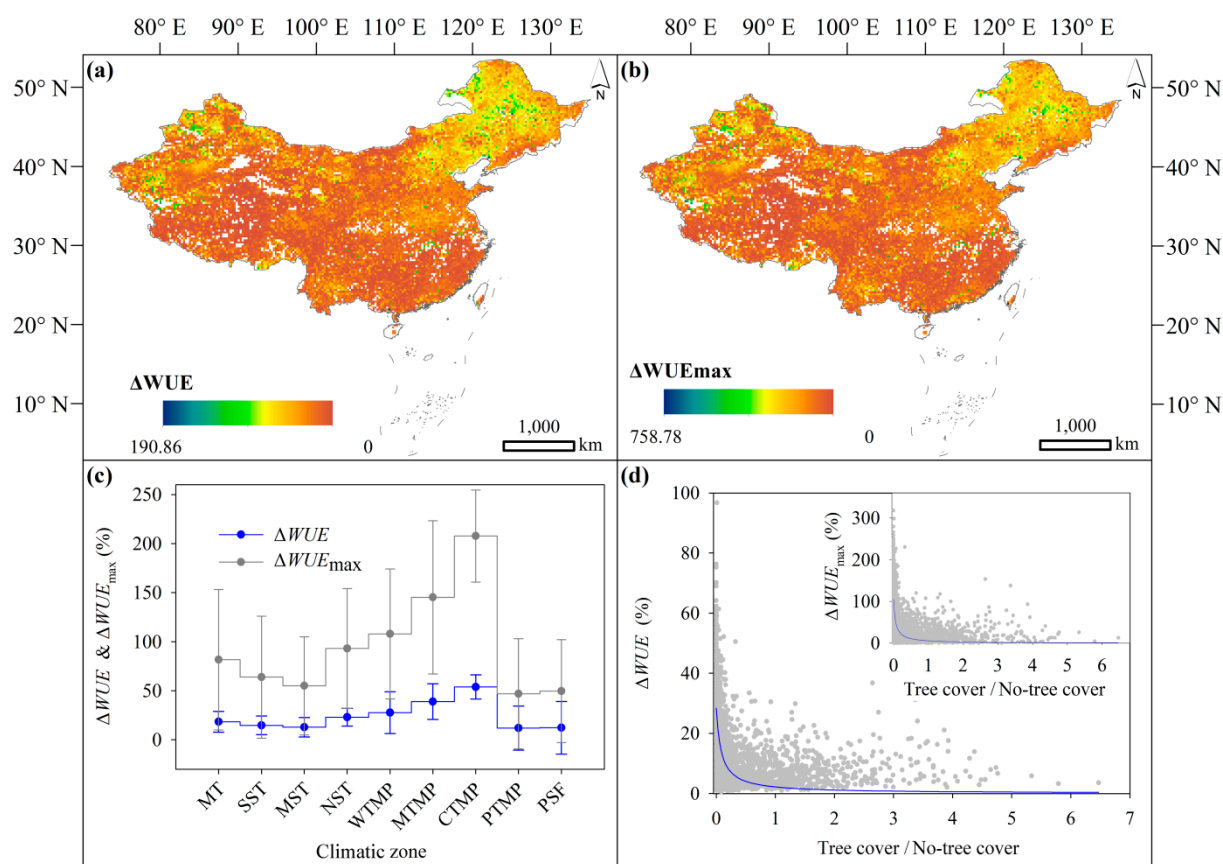

Figure 4. Spatial characteristics of the elasticity coefficient of water use efficiency (*WUE*) to soil moisture (*SM*) change in the growing season of the terrestrial ecosystem in China during 1985–2014. Panels (**a**,**c**,**e**) show the raster map of the sensitivity of *WUE* to *SM* variation via the evapotranspiration (*ET*) and net primary production (*NPP*) pathways and the final effects of both pathways, respectively. Panels (**b**,**d**,**f**) show the sensitivity of *WUE* to *SM* variation via the *ET* pathway and *NPP* pathway and the final effects of both pathways in different climatic zones, respectively. The abbreviations of MT, SST, MST, NST, WTMP, MTMP, CTMP, PTMP, and PSF represent the marginal tropical zone, south subtropics zone, middle subtropics zone, north subtropics zone, warm temperate zone, middle temperate zone, cold temperate zone, temperate zone in Qinghai–Tibet Plateau and the sub-frigid zone in Qinghai–Tibet Plateau (PSF), respectively.

In the *NPP* pathway, the sensitivity coefficient of *WUE* to *SM* ($\frac{\partial WUE}{\partial NPP} \frac{\partial NPP}{\partial \theta}$) had a more apparent spatial variation, and the value ranged from -68.66 to 43.19 with an average of 0.13 (Figure 4c). Thus, *SM* via the *NPP* pathway positively affected *WUE* in 55.71% of the area, whereas it showed a negative influence in the remaining 44.29% of the area. In addition, *SM* via the *NPP* pathway often had a more significant impact (larger absolute value) on *WUE* in the southeast monsoon region and northwestern arid region of China. In different climatic zones (Figure 4d), the impact of *SM* on *WUE* via the *NPP* pathway showed a positive effect in MTMP, WTMP, and PTMP, with elasticity coefficients of 0.74, 0.50, and 0.33, respectively. In contrast, the impacts of *SM* on *WUE* via the *NPP* pathway were negative in the other climatic zones, and the elasticity coefficients ranged from -1.39 to -0.12. Generally, the area percentage of the region in which *SM* had a positive effect on *WUE* via the *NPP* pathway ranged from 28.10% to 63.44% in different climatic zones.

Under the dual effects of *ET* and *NPP* pathways, the final *SM* significantly impacted *WUE*. The elasticity coefficient of *WUE* to *SM* ranged from -74.01 to 39.81, with an average value of -2.87 (Figure 4e). Because the impact of *SM* on *WUE* via the *ET* pathway was completely negative, the comprehensive influence of *SM* on *WUE* also showed a more remarkable negative effect. In the terrestrial ecosystem, *SM* negatively and positively impacted *WUE* in 84.62% and 15.38% of the total area, respectively. For each climatic zone, the average value of the effect of *SM* on *WUE* was also negative, and the negative effect was the most significant in the NST, which had an average elasticity coefficient of -4.27. The average value was the lowest in PTMP, which had an average elasticity coefficient of -1.93. For the other climatic zones, the elasticity coefficient of *WUE* to *SM* ranged from -4.03 to -2.01. Generally, the *NPP* pathway mainly determined the trend of change in *WUE* in different climatic zones, which was because the correlation coefficient between $\frac{\partial WUE}{\partial \theta}$ and $\frac{\partial WUE}{\partial NPP} \frac{\partial NPP}{\partial \theta}$ ($R = 0.84$) was more significant than that between $\frac{\partial WUE}{\partial \theta}$ and $\frac{\partial WUE}{\partial ET} \frac{\partial ET}{\partial \theta}$ ($R = 0.69$). In contrast, the *ET* pathway mostly dominated the influence level (absolute value of the elasticity coefficient of *WUE* to *SM*) of *SM* on the *WUE* (Figure 4b,d,f).

3.4. WUE Variability Caused by SM

In this study, the absolute value of the percentage change in the *WUE* (ΔWUE) was used as an index to analyze the *WUE* variability. Figure 5a shows that the variation of *SM* led to significant *WUE* variability, especially in northeast and northwest China. At the growing season scale, the average ΔWUE due to the variation in *SM* ranged from 0% to 190.86%, with an average value of 28.02% (Figure 5a). For different climatic zones (Figure 5c), *SM* in the CTMP had the most significant effect on *WUE*, causing an average variation in *WUE* of approximately 53.90%. In contrast, *SM* in the PTMP had the least impact on *WUE*, causing only, approximately, a 11.96% variability in *WUE*. For the other climatic zones, ΔWUE caused by *SM* variation in MTMP, WTMP, NST, MT, SST, MST, and PSF were 38.93%, 27.75%, 23.04%, 18.39%, 14.78%, 12.84%, and 12.30%, respectively. The spatial trend of the maximum *WUE* variability (ΔWUE_{max}) was similar to the variability of the ΔWUE (Figure 5b). It also had the greatest change in northeast and northwest China. Furthermore, the ΔWUE_{max} ranged from 0% to 758.78%, with an average value of 109.29%. These results indicated that the maximum change in *SM* over the past 30 years doubled the variability in *WUE*. In different climatic zones, the trend of change in ΔWUE_{max} was the same as that for ΔWUE, but the value of ΔWUE_{max} was larger than that of ΔWUE. ΔWUE_{max} was generally 3.7–4.4 times greater than ΔWUE (Figure 5c).

Figure 5. Percentage change in water use efficiency (Δ*WUE*) caused by soil moisture variation in the terrestrial ecosystem in the growing season. Panels (**a**,**b**) represent the spatial variation characteristics of the Δ*WUE* and Δ*WUE*$_{max}$ of the entire terrestrial ecosystem, respectively. Panel (**c**) represents Δ*WUE* and Δ*WUE*$_{max}$ in different climatic zones. Panel (**d**) shows the scatter plot between the variation in *WUE* and the ratio of tree cover to no-tree vegetation cover. The abbreviations of MT, SST, MST, NST, WTMP, MTMP, CTMP, PTMP, and PSF represent Marginal tropical zone, south subtropics zone, middle subtropics zone, north subtropics zone, warm temperate zone, middle temperate zone, cold temperate zone, temperate zone in Qinghai–Tibet Plateau and the sub-frigid zone in Qinghai–Tibet Plateau (PSF), respectively.

The feedback relationship between *SM* and *WUE* was affected by the climatic factors and vegetation cover. The ratio of vegetation cover between forest and non-forest was also an essential factor affecting the feedback relationship between *WUE* and *SM* (Figure 5d). The lower the forest cover, the more significant the change in *WUE* caused by changes in *SM*. As the forest cover increased, the variability of *WUE* caused by changes in *SM* rapidly decreased. When the cover ratio of forest to non-forest vegetation was higher than one, the variability of the *WUE* caused by changes in the *SM* tended to stabilize. The *WUE* of the forest ecosystem had strong resistance to variation in soil water. In contrast, the *WUE* of non-forest vegetation was more sensitive to the changes in *SM*.

4. Discussion

4.1. The Reliability of Evaluation Results

In most cases, *SM* dominates *ET*, especially in water-limited regions [54,55]. To explore the coupling relationship between *SM* and *ET*, researchers proposed a simple parameterization schematic, in which the *SM* and *ET* of a forest presented a linear relationship [56]. Recently, studies have proposed a conceptual framework for the dependence of the evaporative fraction (*EF*) on *SM*. It is suitable to analyze the soil moisture control on energy partitioning [50,51]. Based on this coupling relationship between *SM* and *EF*, this study established an evaluation framework for the feedback relationship between the *WUE* and *SM*. The uncertainty of this evaluating framework mainly originated from two aspects:

(1) the reliability of the datasets used and (2) the uncertainty of the parameterized expression of *EF* and *SM*.

Previous studies have shown that evaporation, *LE*, *H*, and *SM* data in the GLDAS dataset have good applicability in China [57,58]. Our verification results (Figure 2) also showed that the datasets used in this study were, overall, reliable, despite some overestimation or underestimation. The analysis method for the coupling relationship between *EF* and *SM* has already been applied [51]; however, this framework needs to fit two parameters (namely, θ_c and θ_r), which may cause uncertainty. Given this, the study directly used two determined parameters, namely, θ_f, and θ_r, provided by the dataset of soil hydraulic parameters in China (http://data.tpdc.ac.cn, accessed on 13 May 2020). This study also introduced a dimensionless parameter A. Thus, this study only fit one parameter (A), which could avoid the uncertainty caused by the need to fit two parameters in the original equation and eliminate the error caused by possible overfitting. This study used the monthly *SM* and *EF* data from 1985 to 2000 to fit the multi-year average monthly parameter A. The monthly *SM* from 2001 to 2014 was estimated using Equation (4) and then verified using *SM* data of GLDAS (Figure 2d). The overall trend of change in estimated *SM* was close to the GLDAS *SM* data, and the R^2, RMSE, MAPE, and NSE of this simulation were 0.99, 0.01 $m^3 \cdot m^{-3}$, 18%, and 0.98, respectively. Although there were still some simulation errors, the estimation was generally reliable. Furthermore, the trend of change in the estimated value was consistent with the GLDAS *SM* data; thus, the functional relationship between *SM* and *EF* was credible overall.

4.2. The Coupling Relationship between Soil Moisture and WUE

Studies have shown that *WUE* is sensitive to changing environments [59]. Generally, many factors, such as the CO_2 concentration, nitrogen deposition, climatic factors, vegetation, human drivers, and *SM*, significantly influence *WUE* [6,60–62]. *SM* is one of the critical factors affecting *WUE* [21,63]. However, most studies have not thoroughly explored the mechanisms and accurate quantification of the effects of *SM* on *WUE*. Our results showed that *SM* had a completely negative influence on *WUE* via the *ET* pathway. However, *SM* also directly influenced *WUE* via the *NPP* pathway, which included negative (44.29% of the total areas) and positive effects (55.71% of the total areas); the overall positive effect was dominant. The areas in which *SM* had a negative impact on *WUE* via *NPP* were mainly distributed in the extremely arid desert areas of Northwest China, the cold temperate areas in Northeast China, and humid areas in Southeast China, which might have been caused by the negative impact of *SM* on *NPP* [64].

Under the dual effects of *SM*, there was a clear negative feedback relationship between *WUE* and *SM*, which was generally consistent with existing research [7,31]. The increase in *SM* often led to a decrease in *WUE* in most areas. The strength of the feedback relation between *SM* and *WUE* may have partly depended on the hydrothermal conditions of the local environment. However, the most significant feature of the spatial variability of the *WUE* in this study was that *WUE* showed a downward trend in the arid area of northwestern China. In contrast, there was an upward trend in the humid eastern region of China. Therefore, China's terrestrial ecosystem *WUE* may be more dominated by *ET* than by *NPP* [21]. Because the *NPP* of tropical and subtropical vegetational zones is higher, it is generally approximately 8–10 times that of an arid desert and alpine vegetation areas in northwest China [65]. However, the *WUE* in the tropical and subtropical vegetation zones was smaller than that of the desert and alpine vegetation areas, which may have been due to excessive *ET* reducing the *WUE*. Furthermore, studies have shown that whether the effect of *SM* on *WUE* is positive or negative depends primarily on whether the *ET* or *NPP* process dominates the *WUE* process [21]. This study used the absolute value of $\frac{\partial WUE}{\partial ET} \frac{\partial ET}{\partial \theta}$ and $\frac{\partial WUE}{\partial NPP} \frac{\partial NPP}{\partial \theta}$ to determine which pathway of *ET* or *NPP* dominated the feedback relationship between *SM* and *WUE*. The results showed that the *ET* pathway dominated the feedback relationship between *SM* and *WUE* in 72% of the total area. The region in which the *NPP* pathway determined the feedback relationship only accounted

for approximately 28% of the total area, especially in the Qinghai–Tibet Plateau. Therefore, terrestrial ecosystems can partially offset the influences of soil dryness by improving *WUE*. In addition, this adjustment should be more remarkable in areas where *ET* controls the *WUE* process, such as in the arid regions of the northwest.

4.3. Plausible Changing Trend and Adjustment of WUE

Under the background of climate change, especially with the increase in temperature and drought, the trend of change in *WUE* is uncertain. Studies have shown that a temperature rise would increase the *NPP* of global terrestrial ecosystems [66,67] However, the continuous temperature rise may eventually lead to a significant decrease in *NPP* [51], mainly owing to the limitation of the optimum temperature for plant growth [68,69]. Thus, *WUE* may show two completely different changes in future scenarios of a continuous temperature rise. First, the temperature rise in the early stage could result in a general increase in *NPP*. Meanwhile, the temperature rise in arid areas (water-limited areas) might not contribute much to *ET*, but may cause a linear increase in humid areas [65,66]. Therefore, under the early warming scenario, *WUE* in the arid region of northwestern China could tend to increase significantly. In the humid area, *WUE* may only slightly change. In contrast, in the late warming period, *WUE* in the arid northwestern region may become smaller, owing to the decrease in *NPP*. Correspondingly, the *WUE* in the humid eastern area may decline because of the possible continued increase in *ET*. In addition, future climate changes may lead to an increase in the frequency, intensity, and duration of drought events [70,71]. Therefore, drought will cause a decrease in *SM*, which will affect the trend of change in *WUE*.

Although studies have shown that an ecosystem can respond to increased drought by increasing *WUE* [7,8], this issue may not be straightforward. Because the *WUE* of different vegetation types has various responses to drought, the *WUE* may be positively or negatively correlated with drought and show a quadratic function relationships [59]. In the arid region, the decrease in *SM* caused by drought could lead to a much greater decline in *ET* compared with the change in *NPP* (increasing or decreasing trend) (Figure 4). Finally, a drought may lead to an increase in *WUE* in most areas of the arid region. In humid areas, the energy conditions mainly determine the evaporation process. Therefore, the decline in *SM* in the early drought stage might not cause a significant change in *ET*. At this time, the trend of change in *WUE* might mainly depend on the changing in *NPP*, which could show an upward or downward trend. With the aggravation of drought, *SM* could decrease significantly, which could cause a decline in *ET*. As a result, in the humid area, the original upward trend of *WUE* may be strengthened, and the original downward trend of *WUE* may be stabilized or even reversed in some cases.

To enhance the adaptability of ecosystems to future climate change or mitigate the adverse effects of climate change, it may be necessary to introduce the following suggestions:(1) In arid regions, the existing desert vegetation and grassland should be prevented from shrinking or degrading owing to intense human factors because these vegetation have a high ecosystem resilience [72]. (2) In arid areas with sparse vegetation, greening should be achieved by expanding grassland areas rather than artificial afforestation. C4 plants, which are usually dominated by herbaceous plants, have a higher internal WUE and can better adapt to the natural conditions of limited water and sufficient energy [73]. With the possible aggravation of drought in humid areas, expanding the C4 vegetation area can also be considered.

5. Conclusions

This study developed an analysis framework to quantitatively assess the influence of *SM* on *WUE*. Based on the analysis framework, this paper found that:

(1)   *SM* had an overall negative effect on the *WUE* in the terrestrial ecosystems during the last 30 years. In the *NPP* pathway, *SM* significantly affected *WUE*, and the sensitivity coefficient ranged from −68.66 to 43.19. However, in the *ET* pathway, *SM*

completely negatively affected *WUE*. Under the dual effects of *ET* and *NPP* pathways, *SM* negatively affected *WUE* in 84.62% of the area, whereas it showed a positive influence on *WUE* in the remaining 15.38% of the area. Thus, although *SM* had a positive effect on the *WUE* of individual regions, it still had an overall negative effect on the *WUE* of each climatic zone.

(2) The variation in *SM* could lead to a significant *WUE* variability, especially in Northeast and Northwest China. During the growing season in the past 30 years, the average and maximum variability of *WUE* caused by variation in *SM* were 28.02% and 109.29%, respectively. Regarding different climatic zones, *SM* in CTMP had the greatest effect on *WUE*, whereas it had the least impact on *WUE* in PTMP. In addition, the lower the forest covers, the higher the variability of *WUE* caused by changes in *SM*. The *WUE* of forest ecosystems is more resistant to changes in *SM*, whereas the *WUE* of non-forest vegetation is more sensitive to changes in *SM*.

These findings deepened our understanding of *WUE* changes and their underlying mechanisms, thereby offering important insight for predicting the response of ecosystems to climate change.

Author Contributions: All authors contributed greatly to this work. Conceptualization, X.H.; methodology, X.H.; software, J.Z.; writing—original draft preparation, J.Z. and X.F.; validation, H.H.; formal analysis, X.F. and Y.L.; writing—review and editing, X.H.; project administration, X.H.; funding acquisition, X.H. All authors have read and agreed to the published version of the manuscript.

Institutional Review Board Statement: Not applicable.

Informed Consent Statement: Not applicable.

Data Availability Statement: The GLDAS dataset was obtained from the NASA Global Land Data Assimilation System (GLDAS) Noah model (GLDAS_NOAH025_M_2.0, https://disc.gsfc.nasa.gov/datasets, accessed on 10 October 2020). The monthly net primary productivity (NPP) dataset of China's terrestrial ecosystems in the north of 18°N was obtained from the Global Change Research Data Publishing & Repository of China (http://www.geodoi.ac.cn/WebEn/CategoryList.aspx, accessed on 24 September 2020). The classification dataset of the soil texture (sand, silt, and clay content in 0–100 cm soil depth) and the soil moisture data based on the microwave remote sensing in China during 2002 and 2011 were provided by the "National Tibetan Plateau Data Center" of China (http://data.tpdc.ac.cn, accessed on 13 May 2020). The dataset of soil hydraulic parameters in China was provided by the "National Cryosphere Desert Data Center of China" (http://www.crensed.ac.cn/portal/, accessed on 21 August 2020). The observed *ET* and *NPP* (*NEE*) data in eight flux towers of China were provided by ChinaFLUX (http://www.cnern.org.cn/, accessed on 15 September 2021). The MODIS Land Cover Dynamics Product (MCD12Q2) was obtained from the National Aeronautics and Space Administration (http://modis.gsfc.nasa.gov/, accessed on 16 August 2020).

Conflicts of Interest: The authors declare no conflict of interest.

References

1. Yu, G.; Song, X.; Wang, Q.; Liu, Y.; Guan, D.; Yan, J.; Sun, X.; Zhang, L.; Wen, X. Water-use efficiency of forest ecosystems in eastern China and its relations to climatic variables. *New Phytol.* **2008**, *177*, 927–937. [CrossRef]
2. Aguilos, M.; Stahl, C.; Burban, B.; Hérault, B.; Bonal, D. Interannual and Seasonal Variations in Ecosystem Transpiration and Water Use Efficiency in a Tropical Rainforest. *Forests* **2018**, *10*, 14. [CrossRef]
3. Malone, S.L.; Tulbure, M.G.; Pérez Luque, A.J.; Assal, T.J.; Bremer, L.L.; Drucker, D.P.; Hillis, V.; Varela, S.; Goulden, M.L. Drought resistance across California ecosystems: Evaluating changes in carbon dynamics using satellite imagery. *Ecosphere* **2016**, *7*, e01561. [CrossRef]
4. Wang, L.; Li, M.; Wang, J.; Li, X. An analytical reductionist framework to separate the effects of climate change and human activities on variation in water use efficiency. *Sci. Total Environ.* **2020**, *727*, 138306. [CrossRef]
5. Lavergne, A.; Graven, H.; De Kauwe, M.G.; Keenan, T.F.; Medlyn, B.E.; Prentice, I.C. Observed and modelled historical trends in the water-use efficiency of plants and ecosystems. *Glob. Chang. Biol.* **2019**, *25*, 2242–2257. [CrossRef] [PubMed]

6.	Zhao, J.X.; Feng, H.Z.; Xu, T.R.; Xiao, J.F.; Gueerieri, R.; Liu, S.M.; Wu, X.C.; He, X.L.; He, X.P. Physiological and environmental control on ecosystem water use efficiency in response to drought across the northern hemisphere. *Sci. Total Environ.* **2020**, *758*, 143599. [CrossRef]

7.	Yang, S.; Zhang, J.; Han, J.; Wang, J.; Ron, Y. Evaluating global ecosystem water use efficiency response to drought based on multi-model analysis. *Sci. Total Environ.* **2021**, *778*, 146356. [CrossRef] [PubMed]

8.	Guo, L.; Sun, F.; Liu, W.; Zhang, Y.; Wang, H.; Cui, H.; Wang, H.; Zhang, J.; Du, B. Response of Ecosystem Water Use Efficiency to Drought over China during 1982 2015: Spatiotemporal Variability and Resilience. *Forests* **2019**, *10*, 598. [CrossRef]

9.	Hao, X.; Hao, H.; Zhang, J. Soil moisture influenced the variability of air temperature and oasis effect in a large inland basin of an arid region. *Hydrol. Process.* **2021**, *35*, e14246. [CrossRef]

10.	Yin, D.; Roderick, M.L.; Leech, G.; Sun, F.; Huang, Y. The contribution of reduction in evaporative cooling to higher surface air temperatures during drought. *Geophys. Res. Lett.* **2014**, *41*, 7891–7897. [CrossRef]

11.	Zheng, H.; Lin, H.; Zhou, W.; Bao, H.; Zhu, X.; Jin, Z.; Song, Y.; Wang, Y.; Liu, W.; Tang, Y. Revegetation has increased ecosystem water-use efficiency during 2000–2014 in the Chinese Loess Plateau: Evidence from satellite data. *Ecol. Indic.* **2019**, *102*, 507–518. [CrossRef]

12.	Liu, W.; Sun, F.; Sun, S.; Guo, L.; Wang, H.; Cui, H. Multi-scale assessment of eco-hydrological resilience to drought in China over the last three decades. *Sci. Total Environ.* **2019**, *672*, 201–211. [CrossRef]

13.	Zou, J.; Ding, J.L.; Welp, M.; Huang, S.; Liu, B.H. Assessing the Response of Ecosystem Water Use Efficiency to Drought During and after Drought Events across Central Asia. *Sensors* **2020**, *20*, 581. [CrossRef]

14.	Mokhtar, A.; He, H.; Alsafadi, K.; Mohammed, S.; He, W.; Li, Y.; Zhao, H.; Abdullahi, N.M.; Gyasi-Agyei, Y. Ecosystem Water Use Efficiency Response to Drought over Southwest China. *Ecohydrology* **2021**, e2317. [CrossRef]

15.	He, B.; Wang, H.; Huang, L.; Liu, J.; Chen, Z. A new indicator of ecosystem water use efficiency based on surface soil moisture retrieved from remote sensing. *Ecol. Indic.* **2017**, *75*, 10–16. [CrossRef]

16.	Bai, Y.; Zha, T.; Bourque, C.P.A.; Jia, X.; Ma, J.; Liu, P.; Yang, R.; Li, C.; Du, T.; Wu, Y. Variation in ecosystem water use efficiency along a southwest-to-northeast aridity gradient in China. *Ecol. Indic.* **2020**, *110*, 105932. [CrossRef]

17.	Zhao, J.; Xu, T.; Xiao, J.; Liu, S.; Mao, K.; Song, L.; Yao, Y.; He, X.; Feng, H. Responses of Water Use Efficiency to Drought in Southwest China. *Remote Sens.* **2020**, *12*, 199. [CrossRef]

18.	Huang, L.; He, B.; Han, L.; Liu, J.; Wang, H.; Chen, Z. A global examination of the response of ecosystem water-use efficiency to drought based on MODIS data. *Sci. Total Environ.* **2017**, *601–602*, 1097–1107. [CrossRef] [PubMed]

19.	Jung, M.; Reichstein, M.; Ciais, P.; Seneviratne, S.I.; Sheffield, J.; Goulden, M.L.; Bonan, G.; Cescatti, A.; Chen, J.; de Jeu, R.; et al. Recent decline in the global land evapotranspiration trend due to limited moisture supply. *Nature* **2010**, *467*, 951–954. [CrossRef]

20.	van der Molen, M.K.; Dolman, A.J.; Ciais, P.; Eglin, T.; Gobron, N.; Law, B.E.; Meir, P.; Peters, W.; Phillips, O.L.; Reichstein, M.; et al. Drought and ecosystem carbon cycling. *Agric. For. Meteorol.* **2011**, *151*, 765–773. [CrossRef]

21.	Liu, X.; Feng, X.; Fu, B. Changes in global terrestrial ecosystem water use efficiency are closely related to soil moisture. *Sci. Total Environ.* **2020**, *698*, 134165. [CrossRef] [PubMed]

22.	Wang, C.; Fu, B.; Zhang, L.; Xu, Z. Soil moisture plant interactions: An ecohydrological review. *J. Soils Sediments* **2019**, *19*, 1–9. [CrossRef]

23.	Stocker, B.D.; Zscheischler, J.; Keenan, T.F.; Prentice, I.C.; Pe Uelas, J.; Seneviratne, S.I. Quantifying soil moisture impacts on light use efficiency across biomes. *New Phytol.* **2018**, *218*, 1430–1449. [CrossRef] [PubMed]

24.	Granier, A.; Reichstein, M.; Bréda, N.; Janssens, I.A.; Falge, E.; Ciais, P.; Grünwald, T.; Aubinet, M.; Berbigier, P.; Bernhofer, C.; et al. Evidence for soil water control on carbon and water dynamics in European forests during the extremely dry year: 2003. *Agric. For. Meteorol.* **2007**, *143*, 123–145. [CrossRef]

25.	Tong, X.; Mu, Y.; Zhang, J.; Meng, P.; Li, J. Water stress controls on carbon flux and water use efficiency in a warm-temperate mixed plantation. *J. Hydrol.* **2019**, *571*, 669–678. [CrossRef]

26.	Nie, C.; Huang, Y.; Zhang, S.; Yang, Y.; Zhou, S.; Lin, C.; Wang, G. Effects of soil water content on forest ecosystem water use efficiency through changes in transpiration/evapotranspiration ratio. *Agric. For. Meteorol.* **2021**, *308–309*, 108605. [CrossRef]

27.	Boese, S.; Jung, M.; Carvalhais, N.; Reichstein, M. The importance of radiation for semiempirical water-use efficiency models. *Biogeosciences* **2017**, *14*, 3015–3026. [CrossRef]

28.	Aguilos, M.; Hérault, B.; Burban, B.; Wagner, F.; Bonal, D. What drives long-term variations in carbon flux and balance in a tropical rainforest in French Guiana? *Agric. For. Meteorol.* **2018**, *253*, 114–123. [CrossRef]

29.	Qi, H.; Huang, F.; Zhai, H. Monitoring Spatio-Temporal Changes of Terrestrial Ecosystem Soil Water Use Efficiency in Northeast China Using Time Series Remote Sensing Data. *Sensors* **2019**, *19*, 1481. [CrossRef]

30.	Begum, F.A.; Paul, N.K. Influence of Soil Moisture on Growth, Water Use and Yield of Mustard. *J. Agron. Crop Sci.* **2010**, *170*, 136–141. [CrossRef]

31.	Ahmadi, B.; Ahmadalipour, A.; Tootle, G.; Moradkhani, H. Remote Sensing of Water Use Efficiency and Terrestrial Drought Recovery across the Contiguous United States. *Remote Sens.* **2019**, *11*, 731. [CrossRef]

32.	Liu, L.; Gudmundsson, L.; Hauser, M.; Qin, D.; Seneviratne, S.I. Soil moisture dominates dryness stress on ecosystem production globally. *Nat. Commun.* **2020**, *11*, 1234567890. [CrossRef]

33. Joiner, J.; Yoshida, Y.; Anderson, M.; Holmes, T.; Hain, C.; Reichle, R.; Koster, R.; Middleton, E.; Zeng, F.-W. Global relationships among traditional reflectance vegetation indices (NDVI and NDII), evapotranspiration (ET), and soil moisture variability on weekly timescales. *Remote Sens. Environ.* **2018**, *219*, 339–352. [CrossRef] [PubMed]

34. Talsma, C.J.; Good, S.P.; Jimenez, C.; Martens, B.; Fisher, J.B.; Miralles, D.G.; McCabe, M.F.; Purdy, A.J. Partitioning of evapotranspiration in remote sensing-based models. *Agric. For. Meteorol.* **2018**, *260–261*, 131–143. [CrossRef]

35. Li, X.D.; Shao, M.A.; Zhao, C.L.; Liu, T.; Ma, C.K. Regional spatial variability of root-zone soil moisture in arid regions and the driving factors—A case study of Xinjiang, China. *Can. J. Soil Sci.* **2019**, *99*, 277–291. [CrossRef]

36. Peterson, A.M.; Helgason, W.H.; Ireson, A.M. How spatial patterns of soil moisture dynamics can explain field-scale soil moisture variability: Observations from a sodic landscape. *Water Resour. Res.* **2019**, *55*, 4410–4426. [CrossRef]

37. Potter, C.S.; Randerson, J.T.; Field, C.B.; Matson, P.A.; Klooster, S.A. Terrestrial Ecosystem Production: A Process Model Based on Global Satellite and Surface Data. *Glob. Biogeochem. Cycles* **1993**, *7*, 811–841. [CrossRef]

38. Piao, S.L.; Fang, J.Y.; Guo, Q.H. Application of casa model to the estimation of Chinese terrestrial net primary productivity. *Chin. J. Plant Ecol.* **2001**, *025*, 603–608.

39. Fang, J.Y.; Piao, S.L.; Field, C.B.; Pan, Y.D.; Guo, Q.H.; Zhou, L.M.; Peng, C.H.; Tao, S. Increasing net primary production in China from 1982 to 1999. *Ecol. Environ.* **2003**, *1*, 293–297. [CrossRef]

40. Feng, X.; Liu, G.; Chen, J.M.; Chen, M.; Liu, J.; Ju, W.M.; Sun, R.; Zhou, W. Net primary productivity of China's terrestrial ecosystems from a process model driven by remote sensing. *J. Environ. Manag.* **2007**, *85*, 563–573. [CrossRef]

41. Pei, F.; Li, X.; Liu, X.; Lao, C. Assessing the impacts of droughts on net primary productivity in China. *J. Environ. Manag.* **2013**, *114*, 362–371. [CrossRef]

42. Liang, W.; Yang, Y.; Fan, D.; Guan, H.; Zhang, T.; Long, D.; Zhou, Y.; Bai, D. Analysis of spatial and temporal patterns of net primary production and their climate controls in China from 1982 to 2010. *Agric. For. Meteorol.* **2015**, *204*, 22–36. [CrossRef]

43. Chen, P.F. Monthly NPP Dataset Covering China's Terrestrial Ecosystems at North of 18°N (1985–2015). *J. Glob. Chang. Data Discov.* **2019**, *3*, 34–41.

44. Yang, K.; Watanabe, T.; Koike, T.; Li, X.; Fuji, H.; Tamagawa, K.; Ma, Y.M.; Ishikawa, H. Auto-calibration system developed to assimilate AMSR-E data into a land surface model for estimating soil moisture and the surface energy budget. *J. Meteorol. Soc. Jpn.* **2007**, *85A*, 229–242. [CrossRef]

45. Yang, K.; Chen, Y.; He, J.; Zhao, L.; Lu, H.; Qin, J.; Zheng, D.; Li, X. Development of a daily soil moisture product for the period of 2002–2011 in Chinese mainland. *Sci. China Earth Sci.* **2020**, *63*, 1113–1125. [CrossRef]

46. Yang, K.; Zhu, L.; Chen, Y.; Zhao, L.; Qin, J.; Lu, H.; Tang, W.; Han, M.; Ding, B.; Fang, N. Land surface model calibration through microwave data assimilation for improving soil moisture simulations. *J. Hydrol.* **2016**, *533*, 266–276. [CrossRef]

47. Liu, B.; Henderson, M.; Zhang, Y.; Ming, X. Spatiotemporal change in China's climatic growing season: 1955–2000. *Clim. Chang.* **2010**, *99*, 93–118. [CrossRef]

48. Li, P.; Hu, Z.; Liu, Y. Shift in the trend of browning in Southwestern Tibetan Plateau in the past two decades. *Agric. For. Meteorol.* **2020**, *287*, 107950. [CrossRef]

49. Wang, J.F.; Wang, G.X.; Wang, Y.B.; Li, Y.S. Influences of the degradation of swamp and alpine meadows on CO_2 emission during growing season on the Qinghai-Tibet Plateau. *Chin. Sci. Bull.* **2007**, *52*, 2565–2574. [CrossRef]

50. Schwingshackl, C.; Hirschi, M.; Seneviratne, S.I. Quantifying Spatiotemporal Variations of Soil Moisture Control on Surface Energy Balance and Near-Surface Air Temperature. *J. Clim.* **2017**, *30*, 7105–7124. [CrossRef]

51. Seneviratne, S.I.; Corti, T.; Davin, E.L.; Hirschi, M.; Jaeger, E.B.; Lehner, I.; Orlowsky, B.; Teuling, A.J. Investigating soil moisture–climate interactions in a changing climate: A review. *Earth Sci. Rev.* **2010**, *99*, 125–161. [CrossRef]

52. Nishat, S.; Guo, Y.; Baetz, B.W. Development of a simplified continuous simulation model for investigating long-term soil moisture fluctuations. *Agric. Water Manag.* **2007**, *92*, 53–63. [CrossRef]

53. Wang, B.; Huang, J.; Gong, X. Grid Soil Moisture Constants Estimation based on HWSD over Basin. *J. China Hydrol.* **2015**, *35*, 8–11.

54. Purdy, A.J.; Fisher, J.B.; Goulden, M.L.; Colliander, A.; Halverson, G.; Tu, K.; Famiglietti, J.S. SMAP soil moisture improves global evapotranspiration. *Remote Sens. Environ.* **2018**, *219*, 1–14. [CrossRef]

55. Walker, E.; García, G.A.; Venturini, V.; Carrasco, A. Regional evapotranspiration estimates using the relative soil moisture ratio derived from SMAP products. *Agric. Water Manag.* **2019**, *216*, 254–263. [CrossRef]

56. Brandes, D.; Wilcox, B.P. Evapotranspiration and soil moisture dynamics on a semiarid ponderosa pine hillslope. *Jawra J. Am. Water Resour. Assoc.* **2000**, *36*, 965–974. [CrossRef]

57. Xue, B.L.; Wang, L.; Li, X.P.; Yang, K.; Chen, D.L.; Sun, L.T. Evaluation of evapotranspiration estimates for two river basins on the Tibetan Plateau by a water balance method. *J. Hydrol.* **2013**, *492*, 290–297. [CrossRef]

58. Syed, T.H.; Fa Miglietti, J.S.; Rodell, M.; Chen, J.; Wilson, C.R. Analysis of terrestrial water storage changes from GRACE and GLDAS. *Water Resour. Res.* **2008**, *44*, W02433. [CrossRef]

59. Hao, X.; Ma, H.; Hua, D.; Qin, J.; Zhang, Y. Response of ecosystem water use efficiency to climate change in the Tianshan Mountains, Central Asia. *Environ. Monit. Assess.* **2019**, *191*, 561. [CrossRef] [PubMed]

60. Huang, M.; Piao, S.; Zeng, Z.; Peng, S.; Ciais, P.; Cheng, L.; Mao, J.; Poulter, B.; Shi, X.; Yao, Y. Seasonal responses of terrestrial ecosystem water-use efficiency to climate change. *Glob. Chang. Biol.* **2016**, *22*, 2165–2177. [CrossRef] [PubMed]

61. Hu, Z.; Yu, G.; Fu, Y.; Sun, X.; Li, Y.; Shi, P.; Wangw, Y.; Zheng, Z. Effects of vegetation control on ecosystem water use efficiency within and among four grassland ecosystems in China. *Glob. Chang. Biol.* **2010**, *14*, 1609–1619. [CrossRef]

62. Li, B.; Huang, F.; Chang, S.; Sun, N. The Variations of Satellite-Based Ecosystem Water Use and Carbon Use Efficiency and Their Linkages with Climate and Human Drivers in the Songnen Plain, China. *Adv. Meteorol.* **2019**, *2019*, 8659138. [CrossRef]
63. Garcia, A.; Guerra, L.C.; Hoogenboom, G. Water use and water use efficiency of sweet corn under different weather conditions and soil moisture regimes. *Agric. Water Manag.* **2009**, *96*, 1369–1376. [CrossRef]
64. Su, B.; Shangguan, Z. Decline in soil moisture due to vegetation restoration on the Loess Plateau of China. *Land Degrad. Dev.* **2018**, *30*, 290–299. [CrossRef]
65. Chen, F.; Shen, Y.; Qian, L.; Ying, G.; Xu, L. Spatio-temporal variation analysis of Ecological system NPP in China In past 30 years. *Sci. Geogr. Sin.* **2011**, *31*, 1409–1414.
66. Yu, M.; Wang, G.; Parr, D.; Ahmed, K.F. Future changes of the terrestrial ecosystem based on a dynamic vegetation model driven with RCP8.5 climate projections from 19 GCMs. *Clim. Chang.* **2014**, *127*, 257–271. [CrossRef]
67. Yu, L.; Gu, F.; Huang, M.; Tao, B.; Hao, M.; Wang, Z. Impacts of 1.5 °C and 2 °C Global Warming on Net Primary Productivity and Carbon Balance in China's Terrestrial Ecosystems. *Sustainability* **2020**, *12*, 2849. [CrossRef]
68. Lüdeke, M.K.B.; Dönges, S.; Otto, R.D.; Kindermann, J.; Badeck, F.W.; Ramge, P.; Jäkel, U.; Kohlmaier, G.H. Responses in NPP and carbon stores of the northern biomes to a CO_2-induced climatic change, as evaluated by the Frankfurt biosphere model (FBM). *Tellus* **2010**, *47*, 191–205. [CrossRef]
69. Pei, Y.; Huang, J.; Wang, L.; Chi, H.; Zhao, Y. An improved phenology-based CASA model for estimating net primary production of forest in central China based on Landsat images. *Int. J. Remote Sens.* **2018**, *39*, 7664–7692. [CrossRef]
70. Sun, C.X.; Huang, G.H.; Fan, Y.; Zhou, X.; Lu, C.; Wang, X.Q. Drought Occurring with Hot Extremes: Changes under Future Climate Change on Loess Plateau, China. *Earth's Future* **2019**, *7*, 587–604. [CrossRef]
71. Waseem, M.; Ajmal, M.; Ahmad, I.; Khan, N.M.; Azam, M.; Sarwar, M.K. Projected drought pattern under climate change scenario using multivariate analysis. *Arab. J. Geosci.* **2021**, *14*, 1–13. [CrossRef]
72. Fan, X.; Hao, X.; Hao, H.; Zhang, J.; Li, Y. Comprehensive Assessment Indicator of Ecosystem Resilience in Central Asia. *Water* **2021**, *13*, 124. [CrossRef]
73. Zhang, D.S.; Li, A.L.; Lam, S.K.; Li, P.; Zong, Y.Z.; Gao, Z.Q.; Hao, X.Y. Increased carbon uptake under elevated CO_2 concentration enhances water-use efficiency of C4 broomcorn millet under drought. *Agric. Water Manag.* **2021**, *245*, 106631. [CrossRef]